The Astrophysical Journal, 721:843–855, 2010 September 20 doi:10.1088/0004-637X/721/1/843

MAGIC CONSTRAINTS ON γ-RAY EMISSION FROM CYGNUS X-3

J. Aleksić[1], L. A. Antonelli[2], P. Antoranz[3], M. Backes[4], C. Baixeras[5], J. A. Barrio[6], D. Bastieri[7], J. Becerra González[8,9], W. Bednarek[10], A. Berdyugin[11], K. Berger[11], E. Bernardini[12], A. Biland[13], O. Blanch[1], R. K. Bock[14], A. Boller[13], G. Bonnoli[2], P. Bordas[15], D. Borla Tridon[14], V. Bosch-Ramon[15], D. Bose[6], I. Braun[13], T. Bretz[16], D. Britzger[14], M. Camara[6], E. Carmona[14], A. Carosi[2], P. Colin[14], J. L. Contreras[6], J. Cortina[1], M. T. Costado[8,9], S. Covino[2], F. Dazzi[17,32], A. De Angelis[17], E. De Cea del Pozo[18], B. De Lotto[17], M. De Maria[17], F. De Sabata[17], C. Delgado Mendez[8,33], M. Doert[4], A. Domínguez[19], D. Dominis Prester[20], D. Dorner[13], M. Doro[7], D. Elsaesser[16], M. Errando[1], D. Ferenc[20], M. V. Fonseca[6], L. Font[5], R. J. García López[8,9], M. Garczarczyk[8], M. Gaug[8], N. Godinovic[20], F. Göebel[14,34], D. Hadasch[18], A. Herrero[8,9], D. Hildebrand[13], D. Höhne-Mönch[16], J. Hose[14], D. Hrupec[20], C. C. Hsu[14], T. Jogler[14], S. Klepser[1], T. Krähenbühl[13], D. Kranich[13], A. La Barbera[2], A. Laille[21], E. Leonardo[3], E. Lindfors[11], S. Lombardi[7], F. Longo[17], M. López[7], E. Lorenz[13,14], P. Majumdar[12], G. Maneva[22], N. Mankuzhiyil[17], K. Mannheim[16], L. Maraschi[2], M. Mariotti[7], M. Martínez[1], D. Mazin[1], M. Meucci[3], J. M. Miranda[3], R. Mirzoyan[14], H. Miyamoto[14], J. Moldón[15], M. Moles[19], A. Moralejo[1], D. Nieto[6], K. Nilsson[11], J. Ninkovic[14], R. Orito[14], I. Oya[6], S. Paiano[7], R. Paoletti[3], J. M. Paredes[15], S. Partini[3], M. Pasanen[11], D. Pascoli[7], F. Pauss[13], R. G. Pegna[3], M. A. Perez-Torres[19], M. Persic[17,23], L. Peruzzo[7], F. Prada[19], E. Prandini[7], N. Puchades[1], I. Puljak[20], I. Reichardt[1], W. Rhode[4], M. Ribó[15], J. Rico[1,24], M. Rissi[13], S. Rügamer[16], A. Saggion[7], K. Saito[14], T. Y. Saito[14], M. Salvati[2], M. Sánchez-Conde[19], K. Satalecka[12], V. Scalzotto[7], V. Scapin[17], C. Schultz[7], T. Schweizer[14], M. Shayduk[14], S. N. Shore[25], A. Sierpowska-Bartosik[10], A. Sillanpää[11], J. Sitarek[10,14], D. Sobczynska[10], F. Spanier[16], S. Spiro[2], A. Stamerra[3], B. Steinke[14], J. C. Struebig[16], T. Suric[20], L. Takalo[11], F. Tavecchio[2], P. Temnikov[22], T. Terzic[20], D. Tescaro[1], M. Teshima[14], D. F. Torres[18,24], H. Vankov[22], R. M. Wagner[14], Q. Weitzel[13], V. Zabalza[15], F. Zandanel[19], R. Zanin[1]

(the MAGIC collaboration),

A. Bulgarelli[26], W. Max-Moerbeck[27], G. Piano[28], G. Pooley[29], A. C. S. Readhead[27], J. L. Richards[27], S. Sabatini[30], E. Striani[28], M. Tavani[28,30], and S. Trushkin[31]

[1] IFAE, Edifici Cn., Campus UAB, E-08193 Bellaterra, Spain; roberta@ifae.es
[2] INAF National Institute for Astrophysics, I-00136 Rome, Italy
[3] Università di Siena and INFN Pisa, I-53100 Siena, Italy
[4] Technische Universität Dortmund, D-44221 Dortmund, Germany
[5] Universitat Autònoma de Barcelona, E-08193 Bellaterra, Spain
[6] Universidad Complutense, E-28040 Madrid, Spain
[7] Università di Padova and INFN, I-35131 Padova, Italy
[8] Instituto de Astrofísica de Canarias, E-38200 La Laguna, Tenerife, Spain
[9] Departamento de Astrofisica, Universidad, E-38206 La Laguna, Tenerife, Spain
[10] University of Łódź, PL-90236 Lodz, Poland
[11] Tuorla Observatory, University of Turku, FI-21500 Piikkiö, Finland
[12] Deutsches Elektronen-Synchrotron (DESY), D-15738 Zeuthen, Germany
[13] ETH Zurich, CH-8093, Switzerland
[14] Max-Planck-Institut für Physik, D-80805 München, Germany; tysaito@mpp.mpg.de
[15] Universitat de Barcelona (ICC/IEEC), E-08028 Barcelona, Spain
[16] Universität Würzburg, D-97074 Würzburg, Germany
[17] Università di Udine and INFN Trieste, I-33100 Udine, Italy
[18] Institut de Ciències de l'Espai (IEEC-CSIC), E-08193 Bellaterra, Spain
[19] Instituto de Astrofísica de Andalucía (CSIC), E-18080 Granada, Spain
[20] Croatian MAGIC Consortium, Institute R. Boskovic, University of Rijeka and University of Split, HR-10000 Zagreb, Croatia
[21] University of California, Davis, CA 95616-8677, USA
[22] Institute for Nuclear Research and Nuclear Energy, BG-1784 Sofia, Bulgaria
[23] INAF/Osservatorio Astronomico and INFN, I-34143 Trieste, Italy
[24] ICREA, E-08010 Barcelona, Spain
[25] Università di Pisa and INFN Pisa, I-56126 Pisa, Italy
[26] INAF-IASF, Bologna, Italy
[27] California Institute of Technology, Owens Valley Radio Observatory, Pasadena, CA 91125, USA
[28] Università Tor Vergata and INFN, I-00133 Rome, Italy
[29] Cavendish Laboratory, Cambridge, CB3 0HE, UK
[30] INAF-IASF, I-00133 Rome, Italy
[31] Special Astrophysical Observatory RAS, Nizhnij Arkhyz, Russia
Received 2010 May 3; accepted 2010 July 18; published 2010 September 1

ABSTRACT

Cygnus X-3 is a microquasar consisting of an accreting compact object orbiting around a Wolf–Rayet star. It has been detected at radio frequencies and up to high-energy γ rays (above 100 MeV). However, many models also predict a very high energy (VHE) emission (above hundreds of GeV) when the source displays relativistic persistent jets or transient ejections. Therefore, detecting such emission would improve the understanding of the jet physics. The imaging atmospheric Cherenkov telescope MAGIC observed Cygnus X-3 for about 70 hr between 2006 March

and 2009 August in different X-ray/radio spectral states and also during a period of enhanced γ-ray emission. MAGIC found no evidence for a VHE signal from the direction of the microquasar. An upper limit to the integral flux for energies higher than 250 GeV has been set to 2.2×10^{-12} photons cm^{-2} s^{-1} (95% confidence level). This is the best limit so far to the VHE emission from this source. The non-detection of a VHE signal during the period of activity in the high-energy band sheds light on the location of the possible VHE radiation favoring the emission from the innermost region of the jets, where absorption is significant. The current and future generations of Cherenkov telescopes may detect a signal under precise spectral conditions.

Key words: acceleration of particles – binaries: general – gamma rays: general – methods: observational – X-rays: binaries

Online-only material: color figures

1. INTRODUCTION

Cygnus X-3 is a bright and persistent X-ray binary, discovered in 1966 (Giacconi et al. 1967), but the high-energy processes occurring in the source are still poorly understood. It lies close to the Galactic plane at a distance between 3.4 and 9.8 kpc, probably at 7 kpc, depending on different distance estimates to the Cygnus OB2 association (Ling et al. 2009). The nature and the mass of the compact object are still a subject of debate. Published results suggest either a neutron star of 1.4 $M_\odot$ (Stark & Saia 2003) or a black hole of less than 10 $M_\odot$ (Hanson et al. 2000). The identification of its donor star as a Wolf–Rayet star (van Kerkwijk et al. 1992) classifies it as a high-mass X-ray binary. Nevertheless Cygnus X-3 shows a short orbital period of 4.8 hr, typical of the low-mass binaries, which has been inferred from the modulation of both the X-ray (Parsignault et al. 1972) and infrared emissions (Becklin et al. 1973).

Despite the strong X-ray absorption in this system, which may be caused by the wind of the companion star, the X-ray spectrum has been intensively studied. The source shows two main spectral X-ray states resembling the canonical states of the black hole binaries: the hard state (HS) and the soft state (SS; Zdziarski & Gierlinski 2004; Hjalmarsdotter et al. 2008). The HS is characterized by a weak soft thermal component and a strong non-thermal power-law emission that peaks at hard X-ray energies, whereas the SS, though showing a non-thermal tail (Szostek et al. 2008), is dominated by the optically thick thermal disk emission. In Cygnus X-3, however, the HS displays a high-energy cutoff at ≈20 keV, significantly lower than the ≈100 keV value found for black hole binaries (Hjalmarsdotter et al. 2004; Zdziarski & Gierlinski 2004).

Adding to its peculiarity, Cygnus X-3 is the brightest radio source among the X-ray binaries, quite frequently exhibiting huge radio flares (as intense as few thousand times the quiescent emission level of ∼20 mJy at 1.5 GHz; Braes & Miley 1972), first seen by Gregory et al. (1972). During these outbursts, which occur mainly when the source is in the SS, and last several days, Cygnus X-3 reveals the presence of collimated relativistic jets (e.g., Martí et al. 2001; Mioduszewski et al. 2001; Geldzahler et al. 1983; Miller-Jones et al. 2004). Thus, Cygnus X-3 has been classified as a microquasar. Based on arcsecond-scale radio observations and their relation with soft X-ray emission, six X-ray/radio states have been identified: quiescent (flux densities ∼100 mJy), minor flaring (<1 Jy), suppressed (<100 mJy), quenched (<30 mJy), major flaring (>1 Jy), and post-flaring (Szostek et al. 2008; Tudose et al. 2010; Koljonen et al. 2010). In the transition from the X-ray hard/radio quiescent state to the SS, the radio emission is strongly suppressed, and if it reaches the quenched level, the source usually produces a major radio flare (Waltman et al. 1994).

Cygnus X-3 has also historically drawn a great deal of attention due to numerous claims of detection at TeV and PeV γ rays, using early-days detectors in these energy ranges (Vladimirsky et al. 1973; Danaher et al. 1981; Lamb et al. 1982; Dowthwaite 1983; Samorsky & Stamm 1983; Cawley et al. 1985; Chadwick et al. 1985; Bhat et al. 1986). However, a critical analysis of these observations raised doubts about their validity (Chardin & Gerbier 1989), and in recent years the more sensitive instruments have not confirmed those claims for energies above 500 GeV (Schilling et al. 2001; Albert et al. 2008a). Nevertheless, microquasars are believed to produce a very high energy (VHE) emission inside the jets: high density and magnetic fields provided by the accretion disk and by the companion star create favorable conditions for effective production of γ rays (Levinson & Blandford 1996; Romero et al. 2003; Bosch-Ramon et al. 2006). This radiation could have either an episodic nature due to the ejection of strong radio-emitting blobs (Atoyan & Aharonian 1999), generally occurring in the SS in the case of Cygnus X-3 or a (quasi) stationary character, being originated in the persistent compact jet present during the HS (Bosch-Ramon et al. 2006).

Using data from the Energetic Gamma-Ray Experiment Telescope detector aboard the *Compton Gamma-Ray Observatory*, Mori et al. (1997) reported an average flux of $(8.2 \pm 0.9) \times 10^{-7}$ photons cm^{-2} s^{-1} at energies above 100 MeV coming from the direction of Cygnus X-3. However, no orbital modulation was detected in the signal, precluding a solid association. The experimental situation in the high-energy region has been drastically changed by the results recently published by *AGILE* (Tavani et al. 2009) and *Fermi*/LAT (Abdo et al. 2009). *AGILE* detected the source in five different moments, for a couple of days each, four of them corresponding to the peak emissions shown in the detailed *Fermi*/LAT light curve (see below). The last detection, occurred in 2009 July, has not been published yet by the *AGILE* Collaboration (A. Bulgarelli et al. 2010, in preparation). On the other hand, *Fermi*/LAT detected a clear signal from Cygnus X-3 above 100 MeV during two periods of enhanced activity lasting for several weeks and coinciding with the source being in the SS. The measured flux is variable and shows an orbital modulation, which confirms the origin of the signal from the microquasar. The *AGILE* flux level is comparable with the one of the *Fermi*/LAT flux peaks, as high as 2.0×10^{-6} photons cm^{-2} s^{-1} above 100 MeV.

Observations of binary systems with imaging atmospheric Cherenkov telescopes (IACTs) in the VHE band have proven very fruitful in recent years, with the detection of the orbitally modulated γ-ray emitters PSR B1259-63 (Aharonian et al.

[32] Supported by INFN Padova.
[33] Now at: Centro de Investigaciones Energéticas, Medioambientales y Tecnológicas (CIEMAT), Madrid, Spain.
[34] Deceased.

2005a), LS 5039 (Aharonian et al. 2005b, 2006), and LS I +61 303 (Albert et al. 2006, 2008b, 2009; Acciari et al. 2008, 2009; Anderhub et al. 2009). However, these systems may be different from Cygnus X-3 since the radio and high-energy radiation could be produced in all three sources by the interaction of the winds of a star and an orbiting pulsar (Maraschi & Treves 1981; Tavani & Arons 1997; Dubus 2006). Nevertheless, Cygnus X-3 GeV γ-ray modulation presents some common features to those observed in LS 5039 and LS I +61 303. On the other hand, although observations of other well-established microquasars, such as GRS 1915 + 105 (Acero et al. 2009; Saito et al. 2009), did not reveal any signal, there is an interesting possibility of VHE emission from Cygnus X-1 (Albert et al. 2007a), still to be confirmed by an independent detection. The origin of this possible emission has been speculated to be linked to a maximum of the X-ray super-orbital modulation of the system (Rico 2008). Moreover, there is also a claim by *AGILE* about a Cygnus X-1 detection during a short flare (Sabatini et al. 2010, ATel 2512), which, however, has not been corroborated by *Fermi*/LAT yet.[35] Such experimental results endorsed by theoretical predictions have encouraged deeper observations of the black hole binaries in the VHE band.

This paper reports observations of Cygnus X-3 performed with the Major Atmospheric Gamma Imaging Cherenkov (MAGIC) telescope between 2006 and 2009. All these observations were carried out with the first stand-alone MAGIC telescope, MAGIC phase I. Cygnus X-3 observations were planned to cover different X-ray/radio states, including those that showed a strong high-energy γ-ray flux. This allowed us to search for VHE emission, above 250 GeV, from Cygnus X-3 in the different cases for which this radiation is predicted in theoretical scenarios. In addition, specific analyses were performed to look for predicted features, such as periodic and variable emission. Section 2 describes the performance of MAGIC and the observational strategy. The analysis chain is explained in Section 3. The results obtained by MAGIC in a multi-wavelength context are reported in Section 4. A brief discussion is given in Section 5.

2. OBSERVATIONS

MAGIC (phase I) is an IACT located at the Canary Island of La Palma (Spain), at 28.°8N, 17.°8 W, 2200 m above sea level. It is a 17 m diameter IACT with an energy threshold of 60 GeV (with the standard trigger). The collected Cherenkov light is focused on a multi-pixel camera composed of 576 photomultiplier tubes (PMTs).

The performance of the MAGIC telescope has changed over the years. The largest improvement followed the upgrade of the 300 MHz readout system in 2007 February. The new multiplexed 2 GHz flash analog–digital converters improved the time resolution of the recorded shower images and reduced the contamination of the night sky background (Aliu et al. 2009). Accordingly, the telescope integral flux sensitivity improved from $\approx$2.5% to $\approx$1.6% of the Crab Nebula flux for energies greater than 270 GeV in 50 hr of observations. At these energies, the angular and energy resolutions are $\approx$0.°1 and $\approx$20%, respectively. MAGIC can provide γ-ray point-like source localization in the sky with a precision of $\approx 2'$ (Albert et al. 2008c). It is able to observe under moderate moonlight or twilight conditions (Albert et al. 2007b; Britzger et al. 2009), which, causing an increase of the night sky background, can be monitored through the PMT anode direct currents (DCs).

MAGIC pointed toward Cygnus X-3 for a total of 69.2 hr between 2006 March and 2009 August. Since the source is expected to be variable, the observations were triggered by its state at other wavelengths. In 2006, observations were prompted by flares at radio frequencies. The MAGIC collaboration received two alerts from the RATAN-600 telescope on 2006 March 10 and on 2006 July 26 (S. Trushkin 2006, private communication). Both radio flares had an X-ray counterpart: the source was in the SS according to *RXTE*/ASM and *Swift*/BAT measurements. In 2007, the observations were triggered using public *RXTE*/ASM (1.5–12 keV) and *Swift*/BAT (15–50 keV) data, as follows: (1) *Swift*/BAT daily flux larger than 0.05 counts cm^{-2} s^{-1} and (2) ratio between *RXTE*/ASM and *Swift*/BAT count rates lower than 200. These criteria guaranteed the source to be in the HS. During 2008 and 2009, MAGIC observed Cygnus X-3 following high-energy γ-ray alerts issued by the *AGILE* satellite. The first of these alerts arrived on 2008 April 18, the second one on 2009 July 18 (M. Tavani 2008, 2009, private communication). These last two campaigns occurred when the source was in the SS.

At La Palma, Cygnus X-3 culminates at a zenith angle of 12°. The observations were carried out at zenith angles between 12° and 50°. They were performed partially in an on–off mode and in a false-source tracking mode (wobble; Fomin et al. 1994), the latter pointing to two directions at a distance of 24′ and on opposite sides of the source. The entire Cygnus X-3 data set recorded by MAGIC amounts to 69.2 hr, out of which 12.5 hr[36] were rejected from further analysis because of their anomalous event rates, leading to a total of 56.7 hr of useful data distributed over 39 nights of observation. The details of the observations are quoted in Table 1.

3. DATA ANALYSIS

Data analysis was carried out using the standard MAGIC calibration and analysis software: once the PMT signal pulses are calibrated (Albert et al. 2008d), pixels containing no useful information for the shower image reconstruction are discarded. This is done by an image cleaning procedure which takes into account the amplitude and the timing information of the calibrated signals (Aliu et al. 2009). The constraints on the signal amplitude are increased in the case of moonlight conditions, when the pixel DCs become larger than 2.5 μA (see Table 1). This higher image cleaning allows us to use the standard Monte Carlo (MC) during the analysis of these data, without the need of any correction, as long as the average pixel DCs are below 4 μA (Britzger et al. 2009).

Afterward, the surviving pixels are used to compute the Hillas event image parameters (Hillas 1985). In addition, Hillas and timing variables are combined into a single γ/hadron discriminator (*hadronness*) and an energy estimator by means of the Random Forest classification and regression algorithm, which takes into account the correlation between the different Hillas and timing variables (Breiman 2001; Albert et al. 2008e). These algorithms are trained with a sample of MC-simulated γ-ray events and a sample of background events extracted from real data. The used timing variables allow an improvement of the analysis sensitivity by of a factor of 1.4 (1.2) in data recorded

[35] Preliminary results can be found at http://fermisky.vlogspot.com/2010/03/lat-limit-on-cyg-x-1-during-reported.html

[36] 9.6 hr were rejected due to high-altitude Saharan dust (calima), which affects the atmosphere above Canary islands and is more intense during summer.

Table 1
Cygnus X-3 Observation Log[a]

Obs. Cycle	Date (yyyy mm dd)	(MJD)	Eff. Time (hr)	Zd (°)	DC[b] (μA)	Spectral[c] State
	2006 03 23	53817	0.45	45–50	3.5	
	2006 03 24	53818	0.25	47–50	2.5	
	2006 03 26	53820	0.53	44–50	1.5	
	2006 03 28	53822	0.70	42–50	1.4	
I	2006 03 30	53824	0.80	41–50	1.3	SS
	2006 03 31	53825	0.90	40–50	1.4	
	2006 04 01	53826	1.00	38–50	1.8	
	2006 04 02	53827	0.92	40–50	1.2	
	2006 04 03	53828	1.05	38–50	1.2	
	2006 07 27	53943	3.10	12–34	1.2	
	2006 07 28	53944	2.53	12–31	1.1	
II	2006 07 29	53945	1.73	12–20	1.2	SS
	2006 07 30	53946	1.36	12–20	1.1	
	2006 08 01	53948	0.92	12–20	1.4	
	2006 08 02	53949	1.88	12–19	1.2	
	2007 07 06	54286	2.16	19–45	2.3	
	2007 07 07	54287	4.53	12–45	2.3	
	2007 07 08	54288	1.07	26–45	1.5	
	2007 07 09	54289	0.38	34–40	1.5	
	2007 07 14	54295	1.82	12–21	1.5	
	2007 07 15	54296	1.93	12–21	1.5	
	2007 07 16	54297	1.93	12–21	1.4	
	2007 07 24	54305	1.75	12–23	1.4	
III	2007 07 26	54307	0.98	19–30	1.4	HS
	2007 07 27	54308	0.5	19–30	1.4	
	2007 08 04	54316	0.73	27–35	1.5	
	2007 08 06	54318	2.72	12–30	1.6	
	2007 08 07	54319	1.93	13–31	1.3	
	2007 08 08	54320	1.58	14–31	1.4	
	2007 09 03	54346	1.86	13–37	2.5	
	2008 04 28	54584	0.31	32–40	2.9	
IV	2008 04 29	54585	1.07	24–41	3.2	SS
	2008 04 30	54586	1.33	23–40	2.6	
	2009 07 19	55031	3.48	12–36	1.2	
	2009 07 21	55033	2.21	14–42	1.2	
V	2009 07 22	55034	1.63	12–27	1.1	SS
	2009 08 01	55044	1.81	17–39	1.5	
	2009 08 02	55045	0.88	27–41	1.6	

Notes.
[a] From left to right: observational cycle, date of the beginning of the observations, also in MJD, effective time after quality cuts, zenith angle range, the anode PMT DCs, and the spectral state.
[b] The anode PMT DCs show the level of the moonlight conditions.
[c] Spectral state was derived by using *Swift*/BAT and *RXTE*/ASM data.

with the new ultra-fast (old 300 MHz) readout system (Aliu et al. 2009).

Images with a total charge below 200 photo-electrons were discarded from further analysis in order to homogenize the different data and MC samples and achieve a common stable energy threshold of all the analyses. The number of γ-ray candidates in the direction of the source is estimated by using the distribution of *alpha* angle (Hillas 1985), which is related to the shower orientation. The evaluation of the background depends on the data taking mode. For data taken in the on–off mode in which the signal data sample is called "on" data, the background is estimated using a different sample, called "off" data. The latter has a similar amount of data recorded during the same epoch as the "on" sample at similar zenith angles and atmospheric conditions with no known γ-ray source in the field of view. For the observations carried out in the wobble mode, the background is extracted from three circular control regions, located symmetrically to the source position with respect to the camera center.

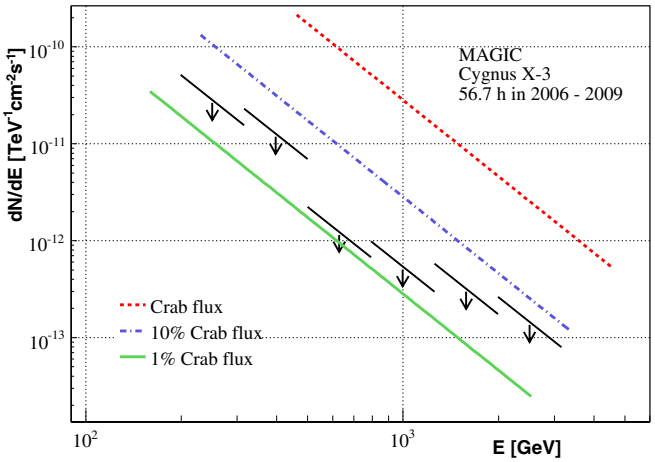

Figure 1. Differential flux ULs at 95% CL for the VHE time-integrated emission. The slope of the arrows indicates the assumed power-law spectrum with a photon index of 2.6.

(A color version of this figure is available in the online journal.)

The Cygnus X-3 data set extends over five different, one-year long cycles of observation, which are characterized by varying performances of the telescope. In addition, cycle I data were recorded in the on–off mode, all the others in the wobble mode, cycle IV data were taken under moderate moonlight conditions.

Each cycle of data was analyzed separately using the appropriate image cleaning procedure and a matching sample of MC-simulated γ-ray events. The analysis selection cuts, on *hadronness* and *alpha*, for each cycle of data were obtained optimizing the sensitivity in a Crab Nebula sample and requiring at least 70% γ-ray selection efficiency. The selected Crab Nebula sample was recorded during the same cycle at similar zenith angles and in the same data taking mode.

All the analyses were then combined in order to calculate the integral flux upper limits (ULs) for energies greater than 250 GeV, which is the energy threshold of each cycle of data. The obtained ULs at the 95% confidence level (CL) were computed following the Rolke et al. (2005) method assuming a Gaussian background and 30% of systematic uncertainties in the flux level (Albert et al. 2008c). The spectrum was assumed to be Crab like (Aharonian et al. 2004), with a photon index of 2.6. However, a 30% change in the photon index yields a variation of less than 1% in the ULs.

4. RESULTS

A search for VHE γ-ray emission from Cygnus X-3 was performed separately for each cycle of observations. None of them yielded a significant excess. The combination of all the data samples yields a 95% CL UL to an integral flux of 2.2×10^{-12} photons cm^{-2} s^{-1} for energies greater than 250 GeV. It corresponds to 1.3% of the Crab Nebula flux at these energies. The differential flux ULs are shown in Table 2 and in Figure 1.

Given that Cygnus X-3 flux is variable at other energy bands on timescales of days, γ-ray signals were also searched for on a daily basis. No significant excess events were found on any observation night. The integral flux ULs for energies above 250 GeV are shown in Table 3 and in the top panel of Figure 2.

In Figure 2, MAGIC results are presented in a multi-wavelength context where the above-mentioned flux variability

Table 2
Differential Flux ULs for the VHE Time-integrated Emission at 95% CL

Energy Range (GeV)	N_{on} Evts.[a]	N_{bg} Evts.[b]	Excess Evts.	Norm. Fact.[c]	Signif.[d] (σ)	UL Evts.[e]	Flux UL (TeV^{-1} cm^{-2} s^{-1})
199–315	4416	4384.5 ± 39.0	31.5 ± 77.0	0.34	0.4	237.8	2.6E−11
315–500	2057	1980.6 ± 28.6	76.4 ± 53.6	0.36	1.5	264.2	1.2E−11
500–792	769	800.8 ± 21.1	−31.8 ± 34.9	0.39	−0.9	51.3	1.1E−12
792–125	289	299.9 ± 12.9	−10.9 ± 21.4	0.38	−0.3	39.2	5.1E−13
1256–1991	102	98.3 ± 6.9	3.7 ± 12.2	0.37	0.5	36.2	3.0E−13
1991–3155	38	32.3 ± 3.5	5.7 ± 7.1	0.35	0.7	27.4	1.3E−13

Notes.
[a] Number of signal events.
[b] Number of normalized background events.
[c] Normalization factor.
[d] Significance.
[e] Maximum number of excess events computed by using Rolke's method.

Table 3
Integral Flux ULs for Energies Above 250 GeV Calculated on a Daily Basis at 95% CL

Date	Time	N_{on} Evts.	N_{bg} Evts.	Excess Evts.	Norm. Fact.	Signif.	UL Evts.	Flux UL	
(MJD)	(hr)					(σ)		(cm^{-2} s^{-1})	(% C.U.)
53817	0.46	42	41.4 ± 1.8	0.6 ± 6.7	0.07	0.1	18.7	1.2E−11	7.5
53818	0.26	43	27.0 ± 0.7	16.0 ± 6.6	0.05	2.8	46.7	5.7E−11	34.2
53820	0.54	85	83.8 ± 4.6	1.2 ± 10.2	0.15	0.1	27.4	1.5E−11	9.3
53822	0.70	132	111.4 ± 3.5	20.6 ± 12.0	0.19	1.7	67.9	2.9E−11	17.4
53824	0.80	84	84.8 ± 2.4	−0.8 ± 9.5	0.15	−0.1	24.3	9.1E−12	5.5
53825	0.80	83	64.3 ± 2.1	18.7 ± 9.3	0.15	2.1	58.0	2.2E−11	13.1
53826	1.00	37	34.3 ± 0.6	2.7 ± 6.1	0.06	0.4	20.9	6.1E−12	3.7
53827	0.92	79	76.5 ± 1.9	2.5 ± 9.1	0.13	0.3	28.4	9.1E−12	5.5
53828	1.05	42	49.3 ± 1.1	−7.3 ± 6.6	0.09	−1.0	10.9	3.1E−12	1.8
53943	3.10	257	274.3 ± 9.5	−17.3 ± 18.6	0.33	−0.9	27.9	4.1E−12	2.5
53944	2.54	232	235.7 ± 8.8	−3.7 ± 17.6	0.33	−0.2	38.6	7.1E−12	4.3
53945	1.73	122	125.7 ± 6.4	−3.7 ± 12.7	0.33	−0.3	27.1	8.4E−12	5.1
53946	1.37	127	108.0 ± 5.9	19.0 ± 12.7	0.33	1.5	65.0	2.5E−11	15.3
53948	0.90	82	65.7 ± 4.6	16.3 ± 10.2	0.33	1.7	54.3	3.2E−11	19.4
53949	1.79	138	143.3 ± 6.9	5.3 ± 13.6	0.33	0.4	42.1	1.3E−11	7.8
54286	2.16	299	314.0 ± 10.2	−15.0 ± 20.1	0.33	−0.74	62.1	1.1E−11	6.8
54287	4.53	547	547.0 ± 13.4	−0.7 ± 27.0	0.33	−0.03	150.3	1.3E−11	8.1
54288	1.07	176	208.0 ± 8.3	−32.0 ± 15.6	0.33	−1.99	20.3	7.0E−12	4.3
54289	0.38	86	84.3 ± 5.3	1.7 ± 10.7	0.33	0.16	41.3	3.9E−11	23.5
54295	1.82	189	176.3 ± 7.6	12.7 ± 15.7	0.33	0.82	76.4	2.1E−11	13.0
54296	1.93	219	209.0 ± 8.3	10.0 ± 17.0	0.33	0.59	74.9	2.0E−11	11.8
54297	1.93	151	138.7 ± 6.7	12.3 ± 14.0	0.33	0.89	65.9	1.7E−11	10.4
54305	1.75	179	167.7 ± 7.4	11.3 ± 15.3	0.33	0.75	111.6	3.1E−11	19.0
54307	0.98	115	117.0 ± 6.2	−2.0 ± 12.4	0.33	−0.16	52.9	2.4E−11	14.5
54308	0.5	71	59.3 ± 4.4	11.7 ± 9.5	0.33	1.27	100.1	8.1E−11	48.8
54316	0.73	85	88.7 ± 5.4	−3.7 ± 10.7	0.33	−0.34	33.0	1.8E−11	11.0
54318	2.72	262	277.3 ± 9.6	−15.3 ± 18.8	0.33	−0.81	39.2	6.7E−12	4.1
54319	1.93	184	184.0 ± 7.8	0.0 ± 15.6	0.33	0.00	61.8	1.5E−11	8.8
54320	1.58	146	152.3 ± 7.1	−6.3 ± 14.0	0.33	−0.95	38.8	1.1E−11	6.8
54346	1.86	182	200.0 ± 8.1	−18.0 ± 15.7	0.33	−1.12	45.3	1.0E−11	6.3
54584	0.31	17	23.0 ± 2.7	−5.0 ± 5.0	0.33	−1.0	8.0	1.0E−11	6.2
54585	1.07	89	75.3 ± 5.0	13.7 ± 10.7	0.33	1.3	50.2	2.0E−11	11.9
54586	1.33	60	66.7 ± 4.7	−6.7 ± 9.1	0.33	−0.7	15.5	5.1E−11	3.1
55031	3.48	186	183.3 ± 7.8	2.7 ± 15.7	0.33	0.2	43.2	5.7E−12	3.4
55033	2.21	71	63.7 ± 4.6	7.3 ± 9.6	0.33	0.8	36.2	7.2E−12	4.4
55034	1.63	50	43.3 ± 3.8	6.7 ± 8.0	0.33	0.9	31.4	9.7E−12	5.8
55044	1.81	88	80.0 ± 5.1	8.0 ± 10.7	0.33	0.8	40.0	9.4E−12	5.7
55045	0.88	69	69.0 ± 4.8	0.0 ± 9.6	0.33	0.0	24.2	1.1E−11	6.6

Note. Refer to Table 2 for the meaning of the columns.

at different energy bands is rather clear. In particular, it displays daily MAGIC VHE integral ULs, high-energy γ-ray (*AGILE* and *Fermi*/LAT (0.1–30 GeV)), hard X-ray (*Swift*/BAT (15–50 keV)), soft X-ray (*RXTE*/ASM (3–5 keV)), and radio measured fluxes from 2006 January 1 (MJD 53736) until 2009 December 15 (MJD 55180). The soft X-ray energy band of *RXTE*/ASM is between 1.5 and 12 keV, out of which only the 3–5 keV band was used, as it yields the cleanest radio/X-

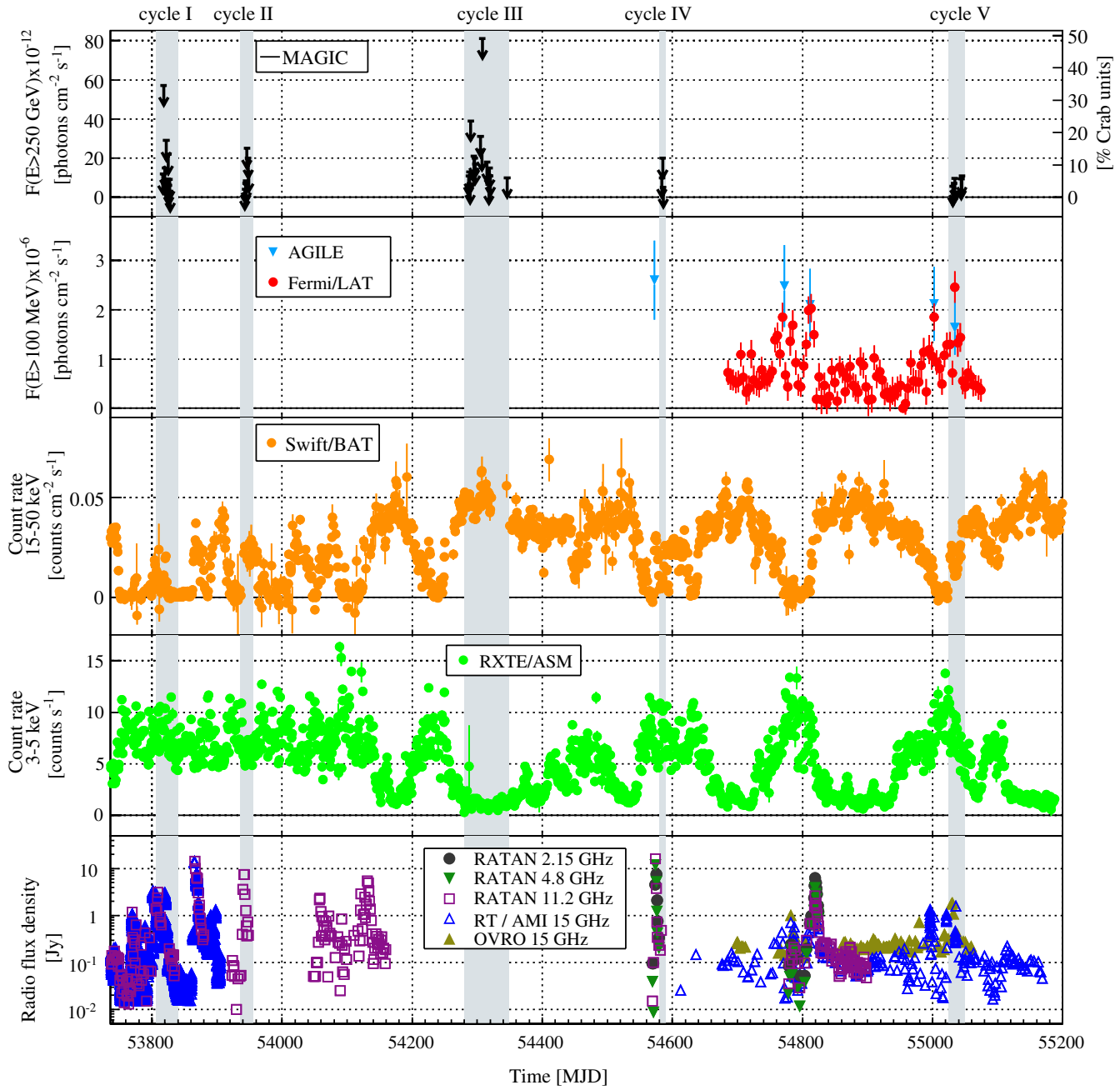

Figure 2. From top to bottom: daily MAGIC VHE integral flux ULs for $E > 250$ GeV, high-energy γ-ray (*AGILE* and *Fermi*/LAT), hard X-ray (*Swift*/BAT), soft X-ray (*RXTE*/ASM), and radio fluxes measured for Cygnus X-3 as a function of time (from 2006 January 1 until 2009 December 15). The gray bands show the periods corresponding to the MAGIC observations. The OVRO and AMI 15 GHz data generally agree well, except for the offset apparent during steady periods which is due to unrelated extended emission resolved by AMI.

(A color version of this figure is available in the online journal.)

ray correlation (Szostek et al. 2008). The radio measurements, displayed in logarithmic scale, were provided by the RATAN-600 telescope at 2.15, 4.8, and 11.2 GHz and by the Ryle telescope (RT), the Arcminute Microkelvin Imager (AMI) telescope, and the Owens Valley Radio Observatory (OVRO) 40 meter telescope at 15 GHz.

The soft and hard X-ray fluxes shown in Figure 2 allow us to derive the X-ray spectral state of Cygnus X-3 during MAGIC observations. Cycle III data are the only ones taken when the source was in the HS, as requested by the observational trigger. All the other observations were carried out when the source was in the SS. The first two MAGIC observational campaigns (cycles I and II) were triggered by flares at radio frequencies, which are expected when the source is in the SS. Unfortunately, the conditions on the trigger together with MAGIC constraints on the observation time did not allow a simultaneous coverage of the flaring states: MAGIC started pointing toward Cygnus X-3 12 and 2 days after the strong radio emission, respectively. On the other hand, in the last observational cycles (IV and V), MAGIC observed the source during the SS, following two *AGILE* alerts on a high-flux activity in the high-energy band: the GeV emission occurs only in this X-ray spectral state. During the second alert, in 2009 July (MJD 55030), MAGIC recorded some data simultaneous with a GeV peak emission and did not detect any VHE signal. This important result will be discussed in detail in Section 4.1.

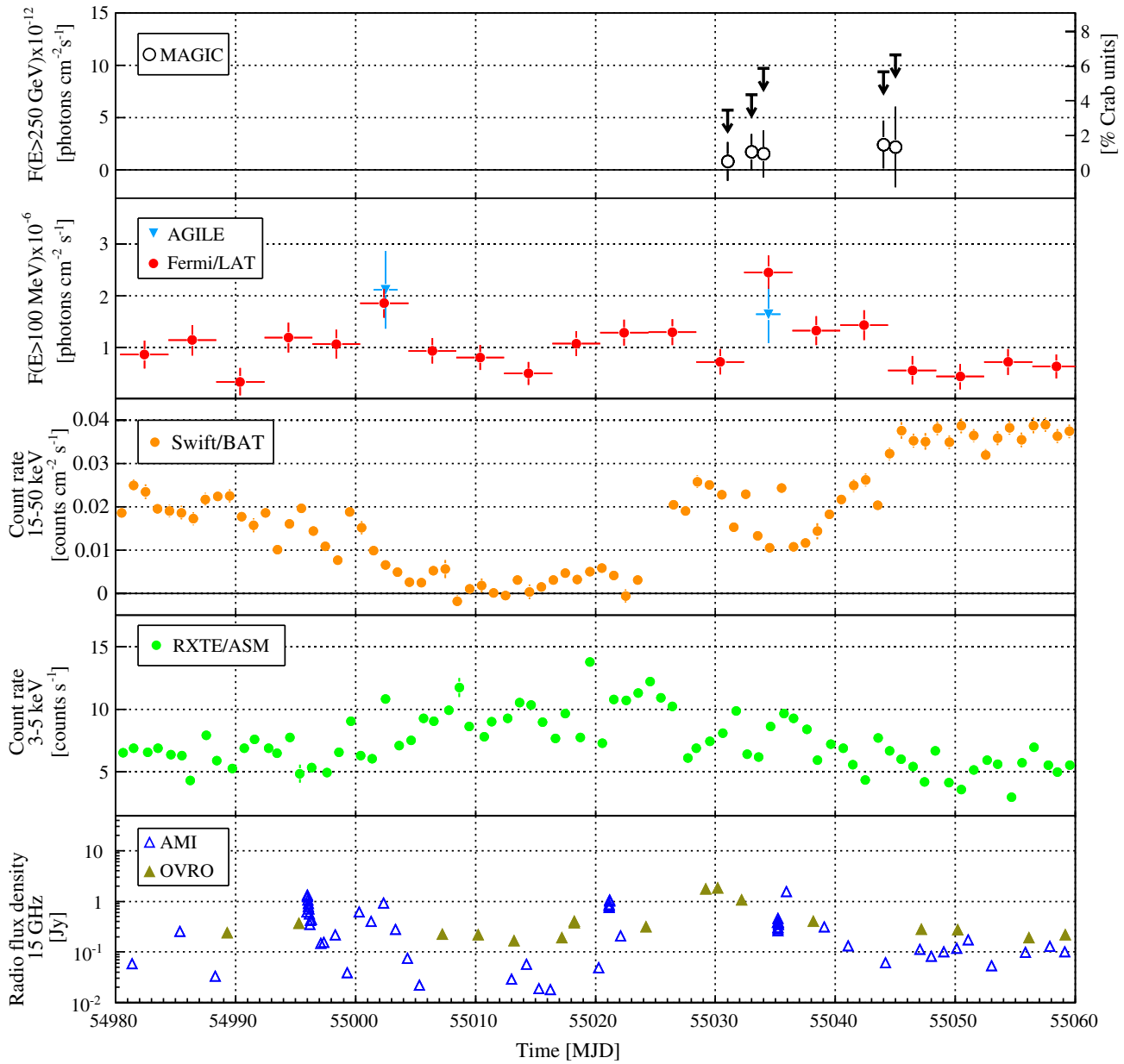

Figure 3. Zoomed view of Figure 2 around the cycle V campaign between 2009 May 29 and August 17. The open circles in the VHE MAGIC panel show the non-significant measured integral fluxes with their statistical error bars (whereas the ULs take into account the systematic errors also).

(A color version of this figure is available in the online journal.)

Microquasars are expected to produce VHE emission inside the jets either when they are compact and persistent, mainly in the HS, or in the presence of strong radio-emitting blobs, which most likely happen during an SS. Therefore, the results of the MAGIC observations were divided according to the X-ray spectral state of the source, as described in Sections 4.2 and 4.3 for the SS and HS, respectively. Besides, in the scenario where the VHE radiation is emitted during powerful synchrotron radio ejections, there might be a correlation between these two wavelengths (Atoyan & Aharonian 1999). Therefore, in Section 4.4 the X-ray/radio states during the MAGIC observations are quoted.

4.1. Results During High-energy γ-ray Emission

Abdo et al. (2009) presented the *Fermi*/LAT observations of Cygnus X-3 between 2008 August 4 and 2009 September 2. They detected a strong signal above 100 MeV, with an overall significance of more than 29 standard deviations, which is mainly dominated by two active periods: MJD 54750–54820 and 54990–55045. These active periods coincide with the X-ray SS of the source, indicating that Cygnus X-3 emits high-energy γ-rays during this spectral state, with an average flux of 1.2×10^{-6} photons cm^{-2} s^{-1} and a photon index of $2.70 \pm 0.05_{\rm stat} \pm 0.20_{\rm sys}$ (under the assumption of a power-law spectrum). They also estimated that the peak flux can be as high as 2×10^{-6} photons cm^{-2} s^{-1} without providing any photon index.

The five *AGILE* detections between 100 MeV and 3 GeV (Tavani et al. 2009; A. Bulgarelli et al. 2010, in preparation) coincide with the strongest high-energy outbursts, which can be seen overlapping with the *Fermi*/LAT light curve. The *AGILE* integral flux averaged over the first four detections is estimated to be 1.9×10^{-6} photons cm^{-2} s^{-1} with a corresponding photon index of 1.8 ± 0.2.

Table 4
Differential Flux ULs for the SS and HS Observations

Spectral State	Energy Range (GeV)	N_{on} Evts.	N_{bg} Evts.	Excess Evts.	Norm. Fact.	Signif. (σ)	UL Evts.	Flux UL (TeV^{-1} cm^{-2} s^{-1})
	199–315	1709	1677.54 ± 24.6	31.5 ± 48.1	0.36	0.7	169.2	3.5E−11
	315–500	926	858.3 ± 18.5	67.7 ± 35.6	0.40	1.9	212.3	1.7E−11
HS	500–792	324	357.5 ± 12.9	−33.5 ± 22.2	0.47	−1.1	30.3	1.2E−12
	792–1256	125	124.9 ± 7.7	0.1 ± 13.6	0.48	0.4	38.0	8.4E−13
	1256–1991	41	33.7 ± 3.9	7.3 ± 7.5	0.46	1.4	32.7	4.5E−13
	1991–3155	14	8.7 ± 1.8	5.3 ± 4.2	0.40	1.3	20.3	1.7E−13
	199–315	2707	2707.0 ± 29.9	0.0 ± 60.0	0.33	0.0	146.2	3.4E−11
	315–500	1131	1122.3 ± 19.2	8.7 ± 38.7	0.33	0.2	108.5	1.1E−11
LH	500–792	445	443.3 ± 12.1	1.7 ± 24.3	0.33	0.1	62.5	3.3E−12
	792–1256	164	175.0 ± 7.5	−11.0 ± 14.9	0.33	−0.7	24.7	7.7E−13
	1256–1991	61	64.7 ± 4.6	−3.7 ± 9.1	0.33	−0.4	18.4	3.7E−13
	1991–3155	24	23.7 ± 2.7	0.3 ± 5.6	0.33	0.1	15.2	1.7E−13

Note. Refer to Table 2 for the meaning of the columns.

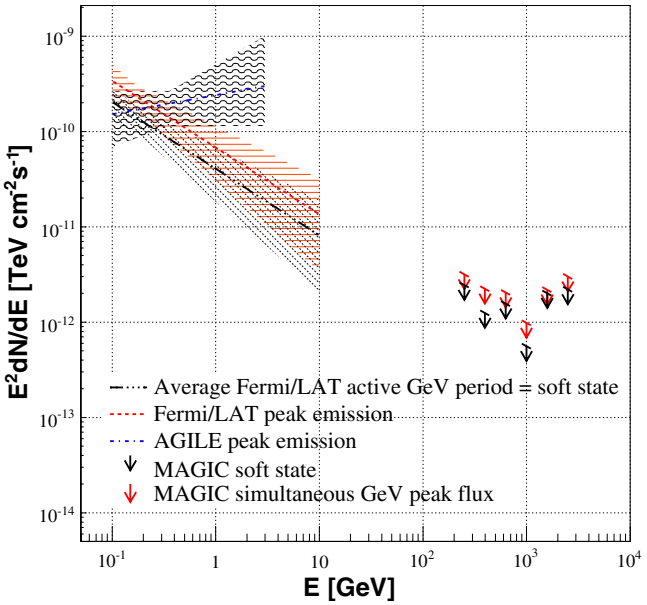

Figure 4. Cygnus X-3 SED in the high-energy and VHE bands. The lines indicate the power-law spectra derived from *Fermi*/LAT and *AGILE* integral fluxes and photon indices, where the corresponding errors were taken into account and are shown in shadowed areas. The arrows display the 95% CL MAGIC differential flux ULs, and their slope indicates the assumed power-law spectrum with a photon index of 2.6. The black indicators show the SED during the period of enhanced GeV activity coinciding with the SS, whereas the colorful ones show it during the high-energy peak emission (MJD 55031–55034).

(A color version of this figure is available in the online journal.)

In cycle V, MAGIC pointed at Cygnus X-3 during the second period of high-energy enhanced activity detected by *Fermi*/LAT, as shown in Figure 3. In particular, MAGIC carried out simultaneous observations with a GeV emission peak on 2009 July 21 and 22 (MJD 55033–55034), and it did not detect any VHE emission. The corresponding MAGIC integral flux ULs above 250 GeV are lower than 6% of the Crab Nebula flux.

Figure 4 shows the spectral energy distribution (SED) of Cygnus X-3 between 100 MeV and 5 TeV including MAGIC 95% CL ULs at VHE, and the power-law spectrum in the high-energy range reported by both *AGILE* and *Fermi*/LAT. The spectra take into account the error in the photon index and in the integral flux, which are 30% and 40% for *Fermi*/LAT and *AGILE*, respectively. The SED for the average SS was obtained considering the average *Fermi*/LAT flux and MAGIC results of the SS data set. On the other hand, to obtain the SED during a high-energy emission peak, the MAGIC measurements simultaneously with the GeV emission peak and both *Fermi*/LAT and *AGILE* spectral power-law fits were used. The *Fermi*/LAT photon index during the peak was assumed to be the same as the one for the SS average flux. The latter being dominated by the brightest phases of the γ-ray outburst, it can also be considered representative of the flaring activity. Both MAGIC ULs are consistent with the extrapolation of the *Fermi*/LAT spectra up to VHE, but not with the extrapolation of the harder *AGILE* spectrum, which would suggest a cutoff between some tens and 250 GeV.

4.2. Results During the Soft State

The MAGIC telescope pointed at Cygnus X-3 when it was in the SS during the observational cycles I, II, IV, and V, corresponding to a total of 30.8 hr. For these observations, soft X-ray measurements in the 3–5 keV band are always above the transitional level set at 3 counts s^{-1} by Szostek et al. (2008).

After having analyzed each data cycle separately, the data sets were combined in order to obtain a global UL to the integral flux for the SS. The UL at the 95% CL for energies greater than 250 GeV is 4.1×10^{-12} photons cm^{-2} s^{-1}, i.e., $\sim 2.5\%$ of the Crab Nebula flux. The differential flux ULs for this spectral state are shown in Table 4 and in the left panel of Figure 5.

Due to the highly anisotropic radiation from the companion star, the predicted γ-ray emission above 250 GeV would be modulated according to the orbital phase (Bednarek 1997). Absorption might play an important role in making the VHE orbital modulation difficult to be detected by the current sensitivity instrumentation (Bednarek 2010). The orbital modulation of the GeV γ-ray emission was detected only when the source was in the SS (Abdo et al. 2009). MAGIC searched for such modulation in this spectral state. A phase-folded analysis was performed assuming the parabolic ephemeris in Singh et al. (2002). The results are shown in the left panel of Figure 6 and in Table 5. No evidence of VHE γ-ray signal was found in any phase bin. The obtained integral flux ULs are smaller than 10% of the Crab Nebula flux for all of them.

4.3. Results During the Hard State

The 25.9 hr of MAGIC cycle III data sample were obtained when Cygnus X-3 was in the HS. *Swift*/BAT count rates during this cycle are rather high, greater than 0.05 counts cm^{-2} s^{-1},

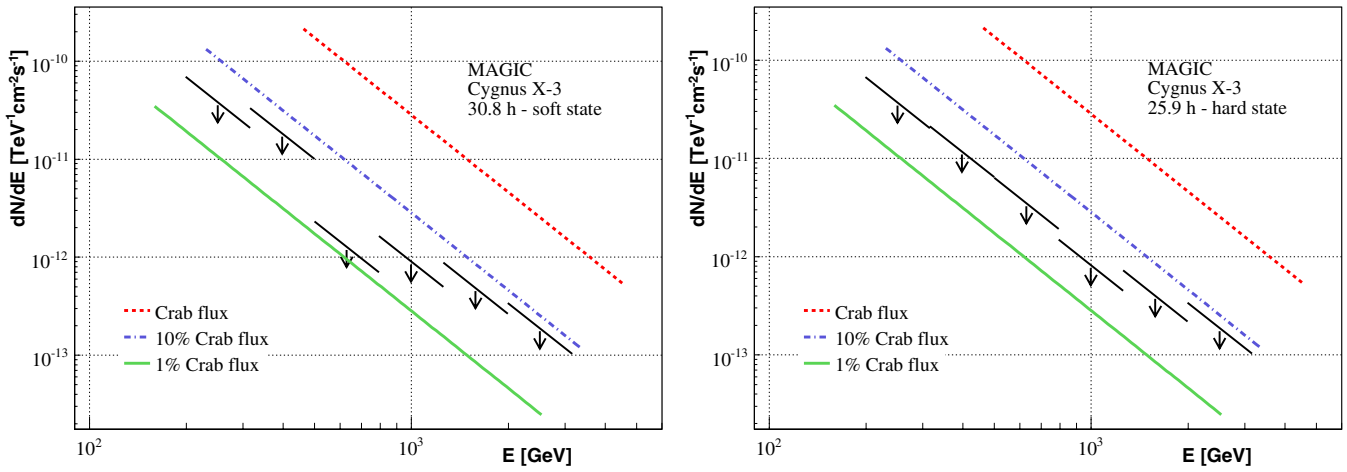

Figure 5. Ninety-five percent differential flux ULs for the SS (left panel) and HS (right panel) observations. The slope of the arrows indicates the assumed power-law spectrum with a photon index of 2.6.

(A color version of this figure is available in the online journal.)

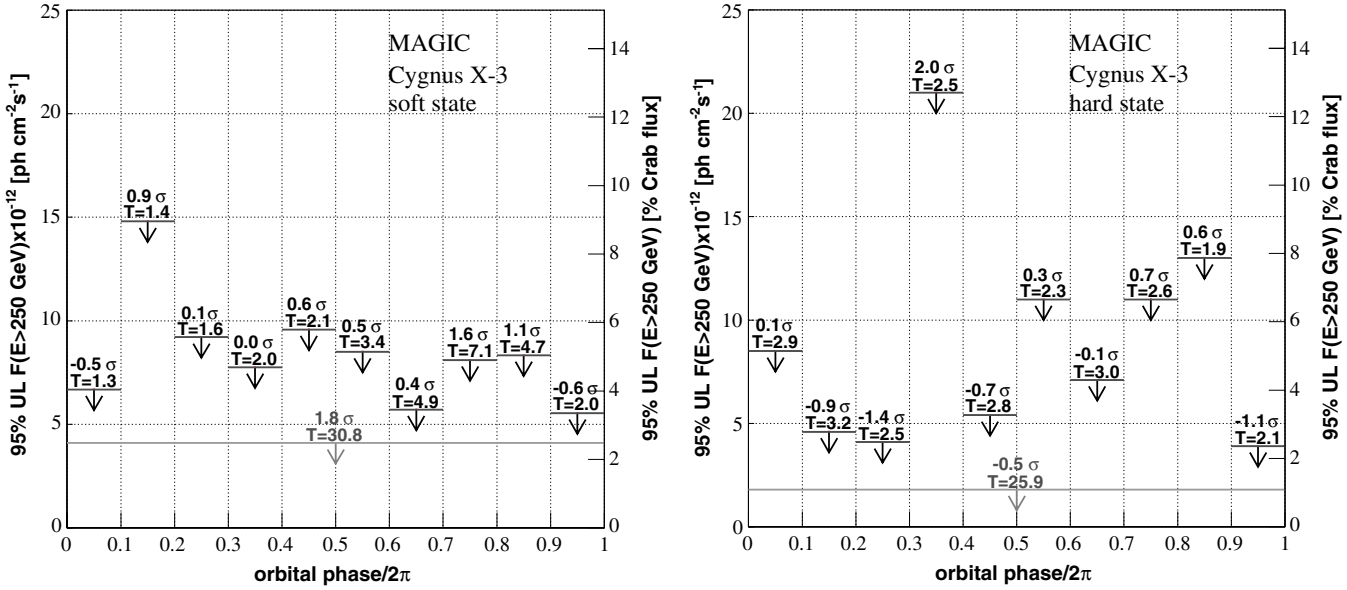

Figure 6. Phase-wise integral flux ULs for $E > 250$ GeV for the SS (left panel) and HS (right panel). The effective observation time (in hours) and the signal significance for each phase bin are written on top of each arrow. The gray arrow indicates the integral flux UL on the VHE time-integrated emission.

whereas the soft X-ray fluxes in the 3–5 keV band are below 2 counts s^{-1}.

For this spectral state, the integral flux UL for energies greater than 250 GeV is 1.1% of the Crab Nebula flux (1.8×10^{-12} photons cm^{-2} s^{-1}). The differential flux ULs are quoted in Table 4 and plotted in the right panel of Figure 5. The performed phase-folded analysis for this spectral state did not yield any significant detection. The computed ULs to the integral flux are, on average, at the level of 5% of the Crab Nebula flux (see the right panel of Figure 6 and Table 5).

4.4. Results During X-ray/Radio States

MAGIC observed Cygnus X-3 in both X-ray main spectral states (see Sections 4.2 and 4.3). However, the state of the source can be further characterized by simultaneous radio flux. Szostek et al. (2008) identified six different X-ray/radio states studying simultaneous observations of the Green Bank Interferometer at 8.3 GHz and *RXTE*/ASM in the energy range 3–5 keV. The relation between these two energy bands is shown in the so-called saxophone plot (see Figure 7). It was noted that the use of other radio frequencies yields similar results. This gives us the confidence that a direct comparison between their and our results using 15 GHz (RT and AMI) and 11.2 GHz (RATAN-600) is reasonable. The OVRO and AMI 15 GHz data generally agree well, but for an ∼0.12 Jy offset apparent during steady periods, probably due to unrelated extended emission resolved out by AMI. Thus, only the AMI 15 GHz were used in this analysis, although our conclusions are not substantially affected by this choice.

Figure 7 shows the soft X-ray (3–5 keV) *RXTE*/ASM count rates versus radio flux densities corresponding either to the nights of MAGIC observations for the five observational cycles or to the *AGILE* flux peaks (only the last four *AGILE* detections were considered since no simultaneous radio data were available for the first one). Unfortunately, no radio data simultaneous with cycle III and cycle IV MAGIC observations were available. Nevertheless, in the case of cycle III data, this does not prevent us from pointing out that Cygnus X-3 was in a quiescent state,

Table 5
Integral Flux ULs for Energies Above 250 GeV for the Phase-folded Analyses of the Observations in the SS and the HS

Spectral State	Phase	Time (h)	N_{on} Evts.	N_{bg} Evts.	Excess Evts.	Norm. Fact.	Signif. (σ)	UL Evts.	Flux UL (cm^{-2} s^{-1})	Flux UL (% C.U.)
	0.0–0.1	1.34	64	68.0 ± 4.7	−4.3 ± 9.3	0.33	−0.5	18.2	6.7E−12	4.0
	0.1–0.2	1.40	75	67.3 ± 4.7	8.3 ± 9.8	0.33	0.9	38.6	1.5E−11	8.9
	0.2–0.3	1.63	108	107.0 ± 5.9	1.3 ± 12.0	0.33	0.1	32.1	9.2E−12	5.6
	0.3–0.4	2.05	162	162.0 ± 7.3	0.3 ± 14.6	0.33	0.0	37.1	7.7E−12	4.7
	0.4–0.5	2.11	113	106.0 ± 5.9	7.3 ± 12.1	0.33	0.6	42.3	9.6E−12	5.8
SS	0.5–0.6	3.40	231	222.3 ± 8.5	8.7 ± 17.5	0.33	0.5	57.1	8.5E−12	5.1
	0.6–0.7	4.93	370	361.3 ± 10.2	9.1 ± 21.8	0.29	0.4	68.3	5.7E−12	3.4
	0.7–0.8	7.13	649	600.7 ± 17.1	49.4 ± 30.7	0.49	1.6	163.9	8.1E−12	4.9
	0.8–0.9	4.69	331	310.0 ± 8.4	21.2 ± 20.0	0.23	1.1	86.4	8.3E−12	5.1
	0.9–1.0	2.05	109	116.0 ± 6.2	−7.0 ± 12.1	0.33	−0.6	22.1	5.5E−12	3.3
	0–1	30.78	2216	2120.3 ± 29.5	96.3 ± 55.5	0.41	1.8	311.6	4.1E−12	2.5
	0.0–0.1	2.89	511	509.7 ± 12.9	1.3 ± 26.1	0.33	0.0	102.5	8.6E−12	5.2
	0.1–0.2	3.23	477	501.3 ± 12.8	−24.3 ± 25.3	0.33	−0.9	52.5	4.6E−12	2.7
	0.2–0.3	2.53	281	308.0 ± 10.1	−27.0 ± 19.5	0.33	−1.4	33.6	4.1E−12	2.5
	0.3–0.4	2.53	266	230.0 ± 8.7	36.0 ± 18.5	0.33	2.0	218.1	2.1E−11	12.4
	0.4–0.5	2.79	248	261.0 ± 9.2	−13.0 ± 18.3	0.33	−0.7	43.2	5.4E−12	3.3
HS	0.5–0.6	2.27	210	205.3 ± 8.2	4.7 ± 16.6	0.33	0.3	73.1	1.1E−11	6.8
	0.6–0.7	2.99	242	243.0 ± 8.9	−1.0 ± 17.9	0.33	−0.1	65.8	7.1E−12	4.3
	0.7–0.8	2.63	234	222.7 ± 8.6	11.3 ± 17.5	0.33	0.6	116.3	1.1E−11	6.8
	0.8–0.9	1.95	199	189.7 ± 7.9	9.3 ± 16.2	0.33	0.6	118.5	1.3E−11	7.8
	0.9–1.0	2.13	235	261.3 ± 9.3	−26.3 ± 17.9	0.33	−1.4	33.8	3.9E−12	2.4
	0–1	25.9	2903	2932.0 ± 31.1	−29.0 ± 62.2	0.33	−0.5	191.0	1.8E−12	1.1

Note. Refer to Table 2 for the meaning of the columns.

just by using the soft X-ray measurements. For cycle IV data, quasi simultaneous radio observations (one day before MAGIC observations) were used. This latter choice does not affect our qualitative result since the source had already entered a post-flaring state. As shown in Figure 8, in 2008 April, *AGILE* detected Cygnus X-3 (MJD 54572–54573) 1 day before a major radio flare (Trushkin et al. 2008) lasting a few days, but MAGIC started pointing at the microquasar 10 days after the peak radio emission.

All the high-energy flux peaks were detected in the right branch of the "saxophone," before, after, or during a flaring state. Although Abdo et al. (2009) quoted a time lag between the radio and the γ-ray peaks of 5 ± 7 days, the correlation between the two energy bands is not yet clear. On the other hand, MAGIC observed Cygnus X-3 in its SS some days after the radio flare occurred (see Figures 8 and 9), although for the first nights of cycle V observations, the radio flux densities are rather high and oscillating between two small flares (see Figure 3).

5. DISCUSSION

MAGIC observations of Cygnus X-3 cover all X-ray spectral states of the source in which VHE emission is thought to be likely produced either from a persistent jet in the HS or during powerful ejections in the SS. However, no significant excess events were found in any of the inspected samples.

VHE γ rays have been predicted from microquasar jets (Atoyan & Aharonian 1999; Romero et al. 2003; Bosch-Ramon et al. 2006). A robust prediction of modeling is that photon–photon absorption cannot be neglected if the γ rays are produced close to a massive star (Bednarek 1997; Orellana et al. 2007). In particular for Cygnus X-3 the presence of a Wolf–Rayet companion, with temperature $T_* \approx 10^5$ K and radius $R_* \approx 10^{11}$ cm, leads to an optical depth $\tau \geqslant 1$ for VHE γ rays for an emitter located at several orbital radii

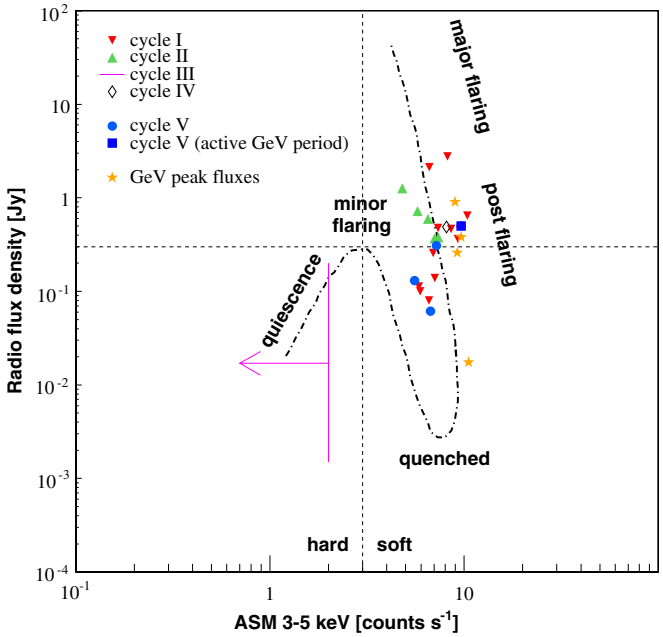

Figure 7. Soft X-ray counts vs. radio fluxes simultaneous with the GeV peak fluxes (yellow stars) and MAGIC observations, where the different marker styles identify the five MAGIC observational cycles. The arrow shows the X-ray flux level during the cycle III MAGIC campaign, for which radio data are not available. Radio measurements are at 11.2 GHz from RATAN-600 and at 15 GHz from RT/AMI. The dot-dashed line shows the expected "saxophone" shape, adapted from Szostek et al. (2008).

(A color version of this figure is available in the online journal.)

from the star (Bednarek 2010). Even under very efficient electromagnetic cascading, i.e., a radiation-to-magnetic energy density ratio $8\pi u_*/B^2 \gg 1$, the expected VHE fluxes are below the sensitivity of the present instruments (Bednarek 2010).

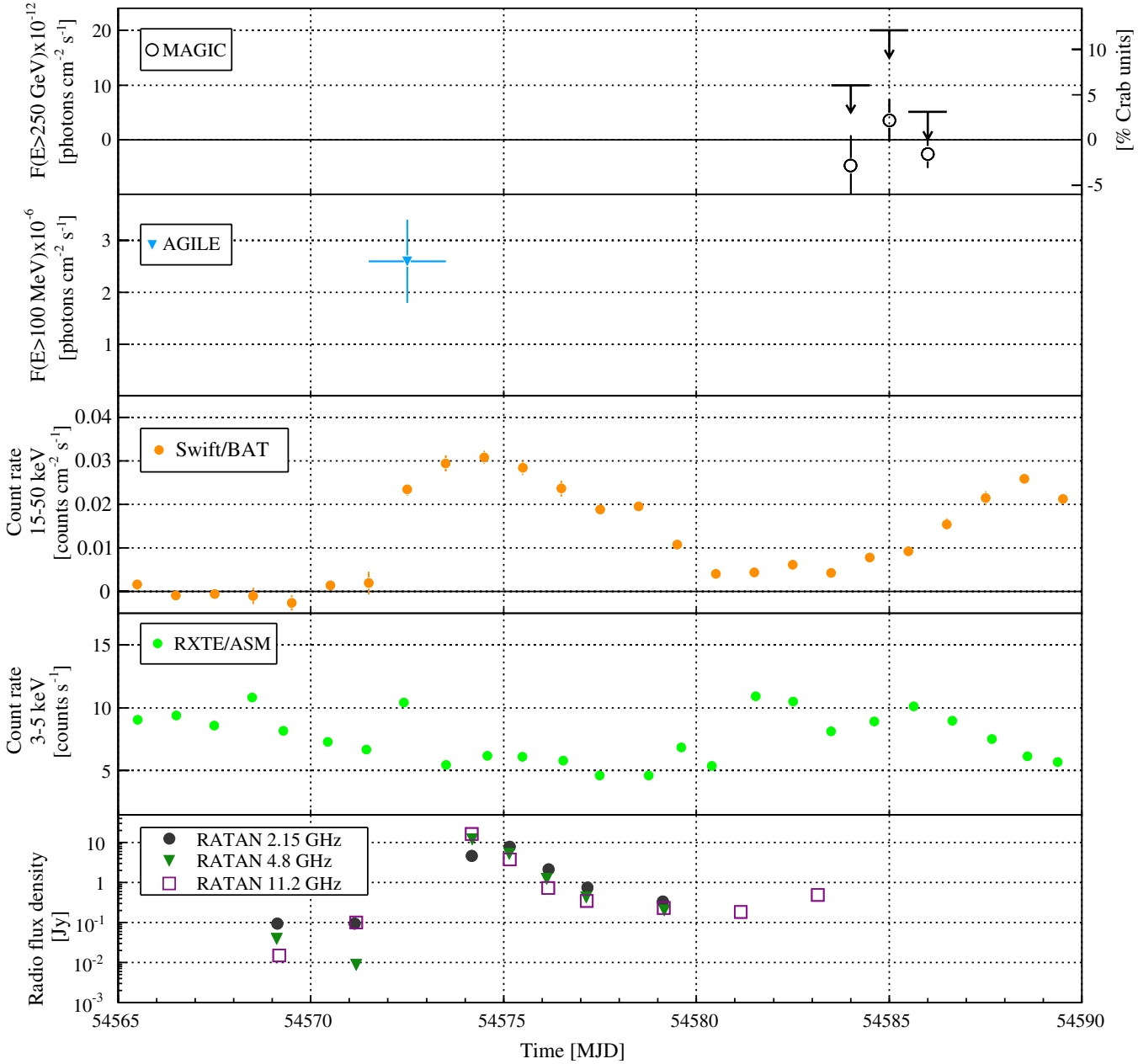

Figure 8. Zoomed view of Figure 2 around the cycle IV campaign between 2008 April 9 and May 2. The open circles in the VHE MAGIC panel show the non-significant measured integral fluxes with their statistical error bars (whereas the ULs take into account the systematic errors also).

(A color version of this figure is available in the online journal.)

Therefore, in order to detect VHE photons, the emitter should be located far from the binary system.

Fermi/LAT detected Cygnus X-3 when it was in the SS and found orbital modulation for the radiation above 100 MeV with a photon index of 2.7 for the periods of enhanced activity (Abdo et al. 2009). For the epochs outside these high-activity periods, the GeV flux decreases significantly (Figure 2 in Abdo et al. 2009) and no modulation is found. The GeV orbital light curve of Cygnus X-3 in the high-energy active periods can be explained in the context of anisotropic inverse Compton scattering with the stellar photons (Abdo et al. 2009; Bosch-Ramon & Khangulyan 2009; Dubus et al. 2010), which is also energetically more efficient than hadronic mechanisms such as *pp* interactions or photomeson production. Since very bright X-ray emission is produced in the inner accretion disk or at the base of the jets in Cygnus X-3, the GeV radiation would be absorbed unless it is originated beyond $\sim 10^{10}$ cm above the compact object. This implies that the GeV radiation is produced in the jet of Cygnus X-3 rather than in the inner accretion disk/corona region. On the other hand, the GeV emitter cannot be too high in the jet, since otherwise there would not be strong orbital modulation (see also Abdo et al. 2009). Therefore, the observed GeV and the predicted detectable VHE emission cannot be explained by one particular population because the former should be produced in/close to the system and the latter farther from it. The location of a hypothetical VHE emitter could coincide with the innermost region of the radio emitting jet, which, to avoid synchrotron self-absorption, should start relatively far from the binary system. This is consistent with the fact that MAGIC did not detect Cygnus X-3 during the high-activity

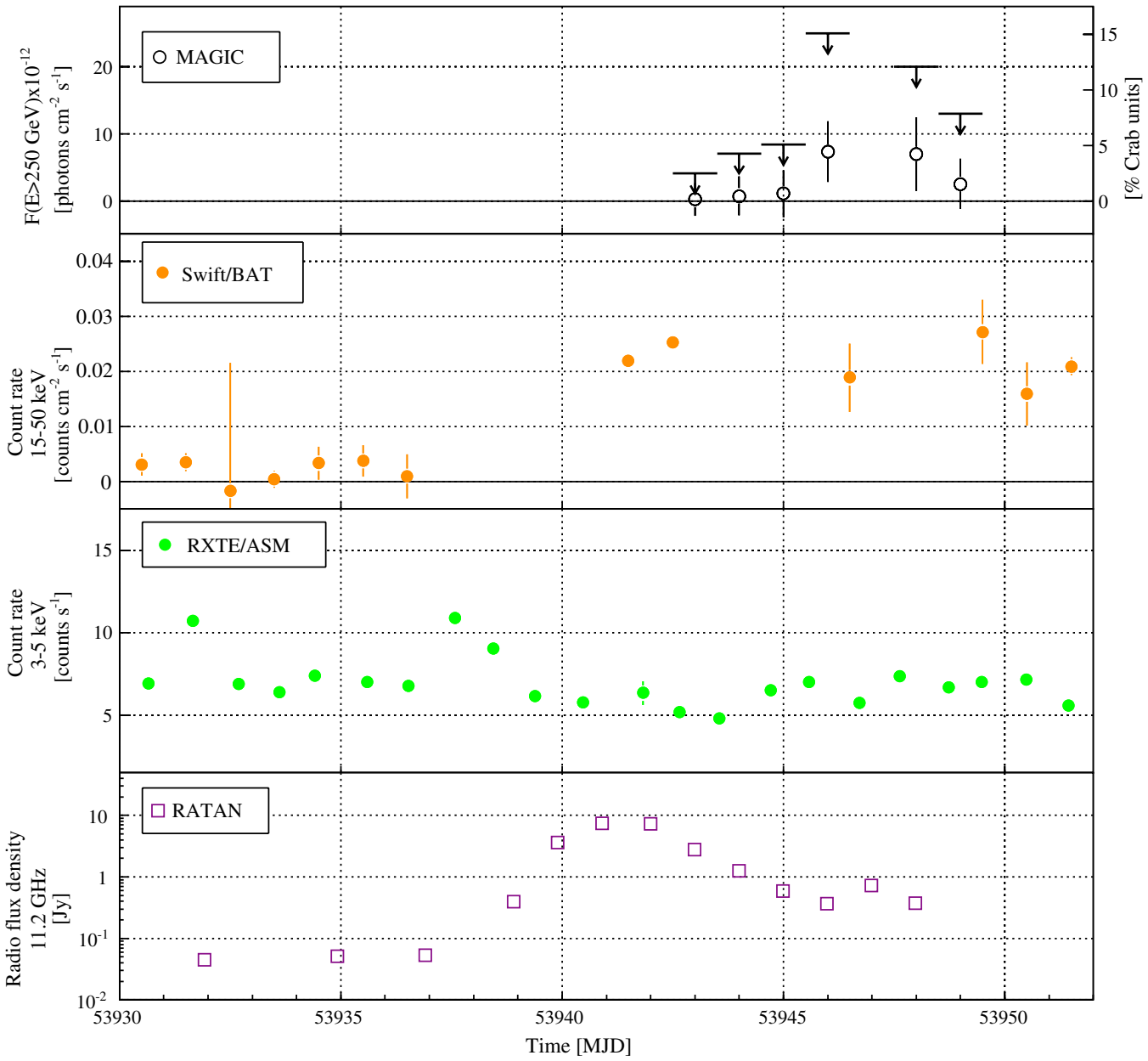

Figure 9. Zoomed view of Figure 2 around the cycle II campaign between 2006 July 14 and August 5. The open circle points in the VHE MAGIC panel show the non-significant measured integral fluxes with their statistical error bars (whereas the ULs take into account also the systematic errors).

(A color version of this figure is available in the online journal.)

GeV period, even though the flux ULs are close to a power-law extrapolation of the *Fermi*/LAT spectrum to energies greater than 100 GeV and well below an extrapolation of the *AGILE* spectrum.

During the periods of GeV high-activity of the source, as by the synchrotron self Compton scenario (Atoyan & Aharonian 1999), a detectable TeV signal could arise during the first hours of a radio outburst. Unfortunately, MAGIC has never observed the source during this phase of the flare, but always some days before or after the maximum radio flux. This radiation would not be strongly modulated due to its origin far from the system. The two times more sensitive two-telescope arrangement, MAGIC phase II, may indeed detect Cygnus X-3 if it observes the source for longer time at the very maximum of a GeV flare, which might be even earlier than the onset of the radio outburst (Abdo et al. 2009).

In the HS, the VHE emission is expected to be produced inside the compact and persistent jets, whose total luminosity is estimated to be at least 10^{37} erg s^{-1} (Martí et al. 2005). The MAGIC VHE γ-ray UL set at 1.1×10^{-12} erg cm^{-2} s^{-1} is equivalent to a VHE luminosity of $\simeq 7 \times 10^{33}$ erg s^{-1} at 7 kpc. Thus, the maximum conversion efficiency of the jet power into VHE γ rays is 0.07% which is similar to that of Cygnus X-1 for the UL on the VHE steady emission, but one order of magnitude greater than that of GRS 1915+105 (Albert et al. 2007a; Acero et al. 2009). These ULs are in good agreement with the theoretical expectations which generally predict a VHE steady luminosity of $\simeq 10^{32}$ erg s^{-1}. Persistent galactic jets do not seem to be good candidate sources to be detected at VHEs by the current sensitivity instrumentation. Only 10 times more sensitive future instruments, such as Cherenkov Telescope Array, may have a chance to detect such VHE emission. This

would provide a new handle on the emission mechanisms of compact jets.

We thank the Instituto de Astrofisica de Canarias for the excellent working conditions at the Observatorio del Roque de los Muchachos in La Palma. The support of the German BMBF and MPG, the Italian INFN, the Swiss National Fund SNF, and the Spanish MICINN are gratefully acknowledged. This work was also supported by the Polish MNiSzW Grant N N203 390834, by the YIP of the Helmholtz Gemeinschaft, and by grant DO02-353 of the Bulgarian National Science Fund. S.T. is grateful for the support of the RATAN observations and the Russian Foundation for Basic Research, grant N08-02-00504-a.

We credit the *Swift*/BAT and *RXTE*/ASM teams for making public their transient monitor and quick-look results, respectively. We also thank Stéphane Corbel for providing useful comments and information on the OVRO and *Fermi*/LAT light curves.

REFERENCES

Abdo, A. A., et al. 2009, Science, 326, 1512
Acero, F., et al. 2009, A&A, 508, 1135
Acciari, V. A., et al. 2008, ApJ, 679, 1427
Acciari, V. A., et al. 2009, ApJ, 700, 1034
Aharonian, F. A., et al. 2004, ApJ, 614, 897A
Aharonian, F. A., et al. 2005a, A&A, 442, 1
Aharonian, F. A., et al. 2005b, Science, 309, 746
Aharonian, F. A., et al. 2006, A&A, 460, 743
Albert, J., et al. 2006, Science, 312, 1771
Albert, J., et al. 2007a, ApJ, 665, L51
Albert, J., et al. 2007b, arXiv:astro-ph/0702475
Albert, J., et al. 2008a, ApJ, 675, L25
Albert, J., et al. 2008b, ApJ, 684, 1351
Albert, J., et al. 2008c, ApJ, 674, 1037
Albert, J., et al. 2008d, Nucl. Instrum. Methods Phys. Res. A, 594, 407
Albert, J., et al. 2008e, Nucl. Instrum. Methods Phys. Res. A, 588, 424
Albert, J., et al. 2009, ApJ, 693, 303
Aliu, E., et al. 2009, Astropart. Phys., 30, 293
Anderhub, H., et al. 2009, ApJ, 706, L27
Atoyan, A. M., & Aharonian, F. A. 1999, MNRAS, 302, 253
Becklin, E. E., Neugebauer, G., Hawkins, F. J., Mason, K. O., Sanford, P. W., Matthews, K., & Wynn-Williams, C. G. 1973, Nature, 245, 302
Bednarek, W. 1997, A&A, 322, 523
Bednarek, W. 2010, MNRAS, 406, 689
Bhat, C. L., Sapru, M. L., & Razdan, H. 1986, ApJ, 306, 587
Bosch-Ramon, V., & Khangulyan, D. 2009, Int. J. Mod. Phys. D, 18, 347
Bosch-Ramon, V., Romero, G. E., & Paredes, J. M. 2006, A&A, 447, 263
Braes, L., & Miley, G. 1972, Nature, 237, 506
Breiman, L. 2001, Mach. Learn., 45, 5
Britzger, D., Carmona, E., Majumdar, P., Blanch, O., Rico, J., Sitarek, J., & Wagner, R. 2009, in Proc. 31st ICRC (Lodz), arXiv:0907.0973
Cawley, M. F., et al. 1985, ApJ, 296, 185
Chadwick, P. M., Dipper, N. A., Dowthwaite, J. C., Gibson, A. I., & Harrison, A. B. 1985, Nature, 318, 642
Chardin, G., & Gerbier, G. 1989, A&A, 210, 52
Danaher, S., Fegan, D. J., & Weekes, T. C. 1981, Nature, 289, 568
Dowthwaite, J. C. 1983, A&A, 126, 1
Dubus, G. 2006, A&A, 456, 801
Dubus, G., Cerutti, B., & Henri, G. 2010, MNRAS, 404, L55
Fomin, V. P., Stepanian, A. A., Lamb, R. C., Lewis, D. A., Punch, M., & Weekes, T. C. 1994, Astropart. Phys., 2, 137
Geldzahler, B. J., et al. 1983, ApJ, 273, L65
Giacconi, R., Gorenstein, P., Gursky, H., & Waters, J. R. 1967, ApJ, 148, L119
Gregory, P. C., et al. 1972, Nature (Phys. Sci.), 239, 114
Hanson, M. M., Still, M. D., & Fender, R. P. 2000, ApJ, 541, 308
Hillas, A. M. 1985, Proc. 19th ICRC (La Jolla), 3, 445
Hjalmarsdotter, L., Zdziarski, A. A., Paizis, A., Beckmann, V., & Vilhu, O. 2004, in Proc. 5th Integral Workshop on the Integral Universe, ed. V. Schönfelder, G. Lichti, & C. Winkler (ESA SP-552; Noordwijk: ESA), 223
Hjalmarsdotter, L., Zdziarski, A. A., Larsson, S., Beckmann, V., Mc-Collough, M., Hannikainen, D. C., & Vilhu, O. 2008, MNRAS, 384, 278
Koljonen, K. I. I., Hannikainen, D. C., McCollough, M. L., Pooley, G. G., & Trushkin, S. A. 2010, MNRAS, 406, 307
Lamb, R. C., Godfrey, C. P., Wheaton, W. A., & Tumer, T. 1982, Nature, 296, 543
Levinson, A., & Blandford, R. 1996, ApJ, 456, L29
Ling, Z., Zhang, S. N., & Tang, S. 2009, ApJ, 695, 1111
Maraschi, L., & Treves, A. 1981, MNRAS, 194, 1
Martí, J., Paredes, J. M., & Peracaula, M. 2001, A&A, 375, 476
Martí, J., et al. 2005, A&A, 439, 279
Miller-Jones, J. C. A., Blundell, K. M., Rupen, M. P., Mioduszewski, A. J., Duffy, P., & Beasley, A. J. 2004, ApJ, 600, 368
Mioduszewski, A. J., Rupen, M. P., Hjellming, R. M., Pooley, G. G., & Waltman, E. B. 2001, ApJ, 553, 766
Mori, M., et al. 1997, ApJ, 476, 842
Orellana, M., Bordas, P., Bosch-Ramon, V., Romero, G. E., & Paredes, J. M. 2007, A&A, 476, 90
Parsignault, D. R., et al. 1972, Nature, 239, 123
Rico, J. 2008, ApJ, 683, L55
Rolke, W., Lopez, A., Conrad, J., & James, F. 2005, Nucl. Instrum. Methods Phys. Res. A, 551, 493
Romero, G. E., Torres, D. F., Kaufman Bernardo, M. M., & Mirabel, I. F. 2003, A&A, 410, L1
Sabatini, S., et al. 2010, ApJ, 712, L10
Saito, T. Y., et al. 2009, Proc. 31st ICRC (Lodz), arXiv:0907.1017
Samorski, M., & Stamm, W. 1983, ApJ, 268, L17
Schilling, M., Mang, O., & Siems, M. 2001, Proc. 27th ICRC (Hamburg), 2521
Singh, N. S., Naik, S., Paul, B., Agrawal, P. C., Rao, A. R., & Singh, K. Y. 2002, A&A, 392, 161
Stark, M. J., & Saia, M. 2003, ApJ, 587, L101
Szostek, A., Zdziarski, A. A., & McCollough, M. 2008, MNRAS, 388, 1001
Tavani, M., & Arons, J. 1997, ApJ, 477, 439
Tavani, M., et al. 2009, Nature, 462, 620
Trushkin, S. A., Nizhelskij, N. A., & Bursov, N. N. 2008, in AIP Conf. Proc. 1053, Observational Evidence for Black Holes in the Universe, ed. S. K. Chakrabarti & A. S. Majumdar (Melville, NY: AIP), 219
Tudose, V., et al. 2010, MNRAS, 401, 890
van Kerkwijk, M. H., et al. 1992, Nature, 355, 703
Vladimirsky, B. M., Stepanian, A. A., & Fomin, V. P. 1973, Proc. 13th ICRC (Denver), 1, 456
Waltman, E. B., Fiedler, R. L., Johnston, K. L., & Ghigo, F. D. 1994, AJ, 108, 179
Zdziarski, A. A., & Gierlinski, M. 2004, Prog. Theor. Phys. Suppl., 155, 99